analytical chemistry

pubs.acs.org/ac Article

Carbon Nanotube Field-Effect Transistor Biosensor for Ultrasensitive and Label-Free Detection of Breast Cancer Exosomal miRNA21

Tingxian Li, Yuqi Liang, Jiahao Li, Yi Yu, Meng-Meng Xiao, Wei Ni,* Zhiyong Zhang,* and Guo-Jun Zhang*

Cite This: *Anal. Chem.* 2021, 93, 15501−15507 Read Online

ACCESS | Metrics & More | Article Recommendations | Supporting Information

ABSTRACT: Tumor-derived exosomal miRNAs may have important functions in the onset and progression of cancers and are potential biomarkers for early diagnosis and prognosis monitoring. Yet, simple, sensitive, and label-free detection of exosomal miRNAs remains challenging. Herein, an ultrasensitive, label-free, and stable field-effect transistor (FET) biosensor based on a polymer-sorted high-purity semiconducting carbon nanotube (CNT) film is reported to detect exosomal miRNA. Different from conventional CNT FETs, the CNT FET biosensors employed a floating gate structure using an ultrathin Y_2O_3 as an insulating layer, and assembled Au nanoparticles (AuNPs) on Y_2O_3 as linkers to anchor probe molecules. A thiolated oligonucleotide probe was immobilized on the AuNP surface of the sensing area, after which miRNA21 was detectable by monitoring the current change before and after hybridization between the immobilized DNA probe and target miRNA. This method achieved both high sensitivity (LOD: 0.87 aM) and high specificity. Furthermore, the FET biosensor was employed to test clinical plasma samples, showing significant differences between healthy people and breast cancer patients. The CNT FET biosensor shows the potential applications in the clinical diagnosis of breast cancer.

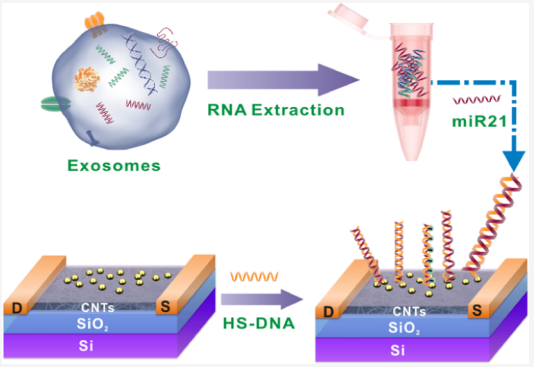

INTRODUCTION

Breast cancer is the most common type of malignant tumor in female cancer diseases worldwide.[1,2] Because of the lack of early diagnosis methods, it is usually late for the disease to be found and difficult to cure, with high mortality.[3,4] Exosomes are cup-shaped vesicles with a phospholipid bilayer secreted by cells. They are involved in tumor cell communication and a variety of biological regulation processes and can even transfer tumor cell genetic material, including messenger RNA (mRNA), microRNA (miRNA), and regulatory small RNA (sRNA).[5−13] Studies have shown that the miRNA expression profile can more accurately aggregate similar tumor types compared to the protein coding mRNA gene expression profile, so exosomal miRNA is also considered as an ideal biomarker for early diagnosis of tumors.[14,15] However, the yield of exosomal miRNA is low when it is isolated from serum or plasma.

The reverse transcription polymerase chain reaction, a molecular diagnostic technique based on nucleic acid amplification, is the most commonly used method for detecting exosomal miRNA.[16] In addition, it is considered as the "gold standard" for miRNA detection. However, its operation is complex and requires the synthesis of cDNA and is easily interfered by other fragments of exosomal miRNA, resulting in great limitations in its detection.[17] In order to achieve sensitive detection of exosomal miRNA without amplification, miRNA detection based on biosensor technologies has been widely studied. Zhao et al.[18] demonstrated that a thermophoretic sensor was used for in situ detection of exosomal miRNA by means of nanoflares, without RNA extraction or target amplification, allowing direct and quantitative measurement of exosomal miRNA down to 0.36 fM in 0.5 μL serum samples. Jiang et al.[19] reported a surface-enhanced Raman scattering sensing platform for in situ detection of exosomal miRNA. On this platform, they prepared locked nucleic acid-modified Au@DTNB, which could enter exosomes and recognize target miRNAs. This method does not require extraction and centrifugation pretreatment, and the detection limit can be as low as 0.21 fM. Yang et al.[20] designed a microfluidic cationic lipid composite nanoparticle (mCLN) assay, in which the cationic lipid composite nanoparticles were used to effectively capture exosomes and dissolve them in situ so as to achieve ultrafast and sensitive detection of exosomal

Received: August 20, 2021
Accepted: October 19, 2021
Published: November 8, 2021

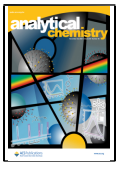

https://doi.org/10.1021/acs.analchem.1c03573
Anal. Chem. 2021, 93, 15501−15507

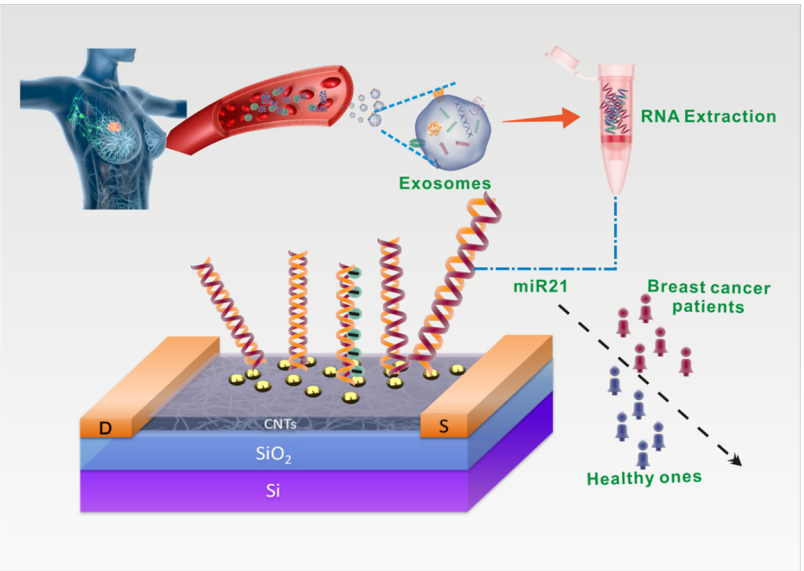

Figure 1. Schematic diagram of ultrasensitive detection of exosomal miR21 using the DNA-functionalized CNT FET biosensor.

RNA. When the platform was used for clinical detection of exosomal miRNA in serum, the required serum volume could be as low as 1 μL. Although these methods can avoid the interference caused by amplification, the labeling or signal amplification is often required to achieve highly sensitive detection. Therefore, simple, amplification-free, label-free, and ultrasensitive detection methods remain to be studied.

A field-effect transistor (FET) biosensor is one of the most promising biosensors in recent years.[21−23] By means of this biosensor, microelectric signals caused by the interaction of biomolecules at the sensing interface can be converted into readable electric signals and amplified by FETs.[24] Since it can achieve high sensitivity detection without any labeling, it has been widely used in the detection of nucleic acids, proteins, and other biomarkers. In addition, they are more attractive because of their small size, low price, and the ability to integrate a large number of sensors on the same chip.[25−28] With an ultrathin body, carbon nanotubes (CNTs) are significantly sensitive to their environment changes with the surface adsorption of various chemicals and biological molecules, so they are considered to be an ideal channel material for FET biosensors.[29−31] CNT FET biosensors have some advantages, just like label-free detection, ultrasensitivity, high miniaturization, and integration. They have been reported to detect various biological species such as DNA, proteins, and cells. To fabricate CNT FET biosensors, usually, an individual CNT or CNT network is employed as the ideal channel material.[32,33] However, due to the influence of the purity and entanglement of CNTs, the large-scale fabrication of the CNT FET biosensors is always attractive.[29,34−37] Moreover, because biological samples are often complex in composition, it is also challenging to maintain good reproducibility caused by the interference of the sample, which limits the real applications of the sensor.[38,39] Very recently, Liang et al.[40] reported a stable and sensitive CNT FET biosensor based on polymer-sorted high-purity semiconducting CNT films and a floating gate (FG) structure using an ultrathin Y_2O_3 as the high κ dielectric layer. The CNT FG-FETs can realize ultrasensitive and label-free detection of DNA sequences and microvesicles, and the detection limits reached as low as 60 aM DNA and 6 particles/mL vesicles. However, the application of semiconductor CNT FETs in the detection of exosomes biomarkers has been even less reported.

In this paper, we report a FET biosensor based on polymer-sorted high-purity semiconducting CNT films and achieve simple, label-free, and ultrasensitive detection of exosomal miRNA (miR-FET). As shown in Figure 1, the CNT FET is fabricated by employing high-purity CNTs as the semiconducting channel between the source and drain electrodes and by growing a Y_2O_3 insulating layer to reduce interference of other interactions. To detect exosomal miRNA (miR21), the corresponding DNA probe is anchored to the surface of gold nanoparticles (AuNPs), which is deposited on the Y_2O_3 interface. When the target miR21 specifically binds to the probe, negative charges are introduced into the sensing interface, resulting in p-type electrostatic doping. The increase of hole carriers in the channel leads to the transfer curve being shifted positively. Tumor exosomes derived from plasma are obtained by high-speed centrifugation, and total exosomal RNA from the plasma samples of clinical healthy individuals and breast cancer patients is extracted for detection. Through the variation of source and drain current I_{ds}, healthy individuals and breast cancer patients can be significantly distinguished, indicating that the sensor has the potential for ultrasensitive detection of exosomal miRNA to achieve early diagnosis of tumors.

EXPERIMENTAL SECTION

Materials and Chemicals. RNaseZap was supplied by Sigma-Aldrich (St. Louis, MO, U.S.A.). Anti-CD63, anti-TSG101, and EpCAM were purchased from Abcam (Cambridge, U.K.). Tris (2-carboxyethyl)-phosphine hydrochloride (TCEP) and 6-mercapto-1-hexanol (MCH) were obtained from Sigma-Aldrich (St. Louis, MO, U.S.A.). Nuclease-free phosphate buffer saline (PBS) and other chemicals were afforded by Generay Biotech Co. Ltd. (Shanghai, China). Ultrapure water, molecular biology-grade, was applied to prepare all buffer solutions throughout the experiments involving hybridization. The ExoQuick-TC Exosome precipitation solution was purchased from System Biosciences (Palo Alto, U.S.A.). The exoRNeasy Serum/Plasma Midi kit was purchased from QIAGEN (Hilden, Germany). The designed

https://doi.org/10.1021/acs.analchem.1c03573
Anal. Chem. 2021, 93, 15501−15507

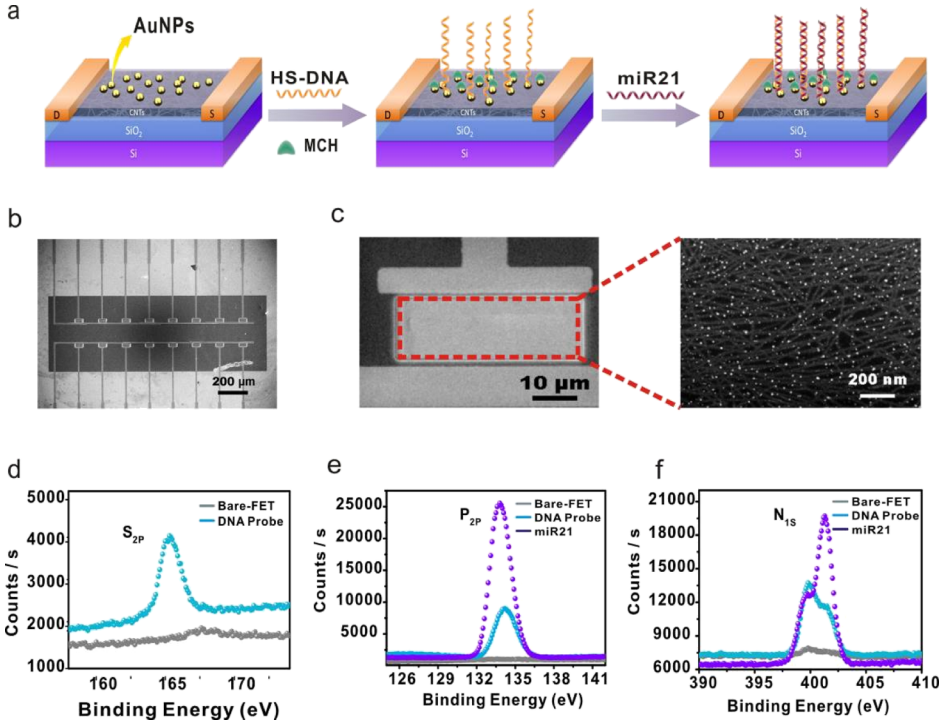

Figure 2. Characterization of DNA immobilization and DNA−miRNA hybridization on the CNT FET sensor surface. (a) Schematic illustration of stepwise DNA probe immobilization and DNA−miRNA hybridization of the CNT FET sensor. (b,c) SEM images of the CNT FET biosensor chip showing the core channel regions (scale bars, 200 μm) and a part of the channel of the device on which AuNPs were uniformly distributed on the Y_2O_3/CNT film (scale bars, 200 nm). (d−f) XPS spectra of S, P, and N elements, respectively.

DNA sequences and all miRNAs were synthesized and purified by Takara Biotechnology (Dalian, China). All the sequences are shown in Table S1. Blood samples of breast cancer patients and healthy donors were provided by the Hubei Provincial Hospital of Traditional Chinese Medicine (Wuhan, China), which was approved by the ethics committee of the hospital.

Device Fabrication. The CNT FET sensor chip was fabricated according to the previous reports.[40] The sorted high-purity CNT solution was diluted using toluene. Si/SiO_2 substrates were immersed in the diluted solution for 48 h. The substrates were then taken out of the solution and then purged with nitrogen. A 3 nm yttrium film was deposited by electron beam evaporation (EBE) and thermally oxidized at 250 °C to combine tightly. A 0.3 nm Au film was deposited by EBE at a rate of 0.1 Å/s to form the AuNPs. The chips were stored in a vacuum-drying oven for subsequent experiments.

DNA Immobilization. The probe DNA sediments were diluted to 10 μM with 1× PBS. The sulfhydryl group (−SH) at one end of DNA was activated with TCEP for 1 h at room temperature. The probe DNA was covalently linked to the AuNPs in the channel by adding 10 μM probe DNA solutions (20 μL) on chip dropwise and incubating for 12 h. These chips were then washed with 1× PBS and deionized water repeatedly to remove the excess probe DNAs, which were nonspecifically adsorbed in the channel. Subsequently, 1 mM MCH was added to the channel of the chips for 2 h to block the excess reactive groups remaining on the Au surface. The obtained device could be applied to subsequent detection.

Detection of Exosomes miRNA21. The chip surface was treated with RNaseZap before hybridization with RNA. For exosomal miR21 detection, 20 μL of target miRNA prepared with nuclease-free PBS was incubated with the DNA-functionalized sensor chip at 37 °C for 1 h. Then, the chip was washed with nuclease-free water and dried with nitrogen flow.

Exosome Isolation and RNA Extraction. Cell-derived exosomes were extracted using the ExoQuick-TC exosome precipitation solution (System Biosciences, America). Plasma exosomes were isolated according to the recommended protocol of exoRNeasy Serum/Plasma Midi kit (QIAGEN, Germany). Exosomal total RNA was further extracted by exoRNeasy Serum/Plasma Midi kit (QIAGEN, Germany).

Electrical Measurement. The measurement system consisting of a probe station (EverBeing BD-6) and a semiconductor characterization system (Keithley 4200-SCS) was used. All measurements regarding the electrical characterization of the FET devices were conducted with a liquid gate at room temperature. When the exosomal miR21 was hybridized with the DNA probe on the chip, the electrical transfer curves were recorded by sweeping the electrolyte gate voltage V_g while fixing V_{ds} at −0.1 V (I_{ds} is the drain current, V_g is the gate voltage, and V_{ds} is the drain voltage). The target miRNA carrying negative charge was introduced into the sensing interface, resulting in p-type electrostatic doping, and the transfer curve shifted positively.

RESULTS AND DISCUSSION

Design and Characterization of miR-FET. The stepwise process of DNA probe immobilization and DNA−miRNA hybridization on the sensing interface is diagrammed in Figure 2a. The thiolated DNA probe binds to AuNPs via the Au−S bond. Then, MCH is used to block the unbound AuNPs to reduce the nonspecific adsorption. Finally, miRNA is hybridized to the immobilized DNA molecules. The scanning electron microscopy (SEM) image shows the CNT FET chip structure. Each chip contained 16 sensing channels (Figure 2b)

https://doi.org/10.1021/acs.analchem.1c03573
Anal. Chem. 2021, 93, 15501−15507

in which a network of high-purity semiconductor CNTs was used as the channel material between the source and drain, and the Y_2O_3 insulation layer and AuNPs were deposited later on. The SEM image shows that the AuNPs were uniformly and compactly distributed on Y_2O_3 (Figure 2c). Then, the DNA modification and DNA−miRNA hybridization were further characterized by X-ray photoelectron spectroscopy (XPS) (Figure 2d−f). After the HS-DNA probe was functionalized on the AuNP surface, S_{2p}, P_{2p}, and N_{1s} peaks appeared at 164.5, 134.4, and 399.8 eV, respectively, indicating that DNA has been immobilized as anticipated. As described in Figure 2e,f, the sharp increment of P_{2p} (134.4 eV) and N_{1s} (399.8 eV) peaks after miR21 hybridization corroborated that the DNA−miRNA hybridization was successful. In addition, energy-dispersive X-ray spectroscopy analysis of the bare-FET chip (bare-FET), DNA modification chip (DNA probe), and DNA−miRNA hybridization chip (miR21) to confirm the chemical elements in the channels. As shown in Figure S1, the EDS analysis results indicate that all chips included Si, O, C, and Au elements because the chips consisted of the substrate Si, SiO_2, CNTs, and the AuNPs. S, P, and N elements appeared on the DNA modification chip, indicating that HS-DNA probes were successfully immobilized on the AuNPs surface through Au−S bonds. Much more amounts of P and N elements appeared on the DNA−miRNA hybridization chip, further verifying that target miR21 was successfully hybridized with the DNA probe.

$I_d - V_g$ transfer curves of the DNA functionalization and hybridization process shown in Figure S2 further confirmed the successful construction of miR-FET. The sensor is a p-type device, which conducts electricity mainly through hole carriers. When the DNA probe was immobilized on the AuNP surface, a large amount of negative charges carried by the DNA was introduced into the sensing interface of the sensor, resulting in an electrostatic gating effect, thereby generating an electrostatic gating effect. The increase of hole carriers between the source and drain led to the increase of source and drain current I_{ds}. When the target miRNA was specifically hybridized to the probe, further negative charges were introduced, and the transfer curves further shifted positively.

Sensitivity. In order to explore the sensitivity of the CNT FET biosensor for detecting exosome miRNA, we applied a series of target miRNA21 with known concentrations in buffer solution to the DNA-functionalized CNT FET chips and used the measurement system to conduct electrical measurements for recording the corresponding $I_d - V_g$ curve. We chose miR21 as the detection target because it has high expression in the breast cancer-related exosomes, and it is considered to have potential as a biomarker for early diagnosis of breast cancer. As shown in Figure 3a, as the concentration of target miR21 increased from 0 to 1 nM, the negative charges also increased with the concentration, and the transfer characteristic curves also shifted positively. We quantified the response of the CNT FET sensor to the different concentrations of miRNA 21 by calculating the change value of I_{ds} before and after the hybridization, $\Delta I_{ds} = I_{ds} - I_0$, in the case of $V_{ds} = -0.1$ and $V_g = -0.7$ V. As shown in Figure 3b, the ΔI_{ds} response shows a wide linear range (1 aM to 1 nM) and has a good linear relationship with the logarithmic concentration (correlation coefficient 0.996). The corresponding equation is $\Delta I_{ds} = 0.1408\lg C_{miR21} + 2.9066$. The LOD was calculated to be 0.87 aM based on the $3\sigma/S$ rule (σ represents the standard deviation of the blank signal; S is the slope). We detected miR21 at different

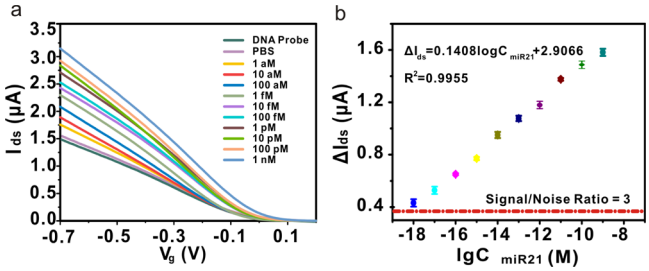

Figure 3. Sensitivity. (a) Transfer curve evolution of the CNT FET biosensors recorded after the introduction of various miRNA 21 concentrations ranging from 1 aM to 1 nM. All measurements were carried out in 0.01× PBS electrolyte. $V_{ds} = -0.1$ V. (b) Calibration curves at a series of miR21 concentrations ($n = 5$). The dashed line refers to threefold noise level.

concentrations from 1 aM to 1 nM, in which each concentration was tested 5 times with a sensor. The relative standard deviation was found to range from 0.3 to 3.7% (Figure S3).

Compared to other sensing platforms, this sensor is one of the most sensitive biosensors currently used for the detection of exosomal miRNA (Table S1). It should be noted that the sensor does not require a signal amplification strategy. Its high detection sensitivity is due to adoption of a FG FET structure in which the conduction channel is isolated from the solution by an ultrathin Y_2O_3 insulator. Moreover, usage of AuNPs amplifies the detection signals by capturing more DNA probes and target miRNAs. Compared with some other sensors constructed by the signal amplification strategy, such as rolling circle amplification, strand displacement amplification, catalytic hairpin assembly amplification, and polymerase-assisted signal amplification, the detection principle and operation steps of this sensor are simple and scalable.

Specificity. After confirming that the CNT FET biosensor can detect miRNAs sensitively, we investigated the sensor's specificity by applying fully complementary sequences (miRNA21), single-base mismatch sequences (SM) at different locations, three-base mismatch sequences (TM), and random mismatch sequences (miRNA10b) to the DNA-functionalized CNT FET chips. As shown in Figure 4a, the signal responses ΔI_{ds} induced by SM-a (1 pM), SM-b (1 pM), SM-c (1 pM), TM (1 pM), and miR10b (random sequence, 1

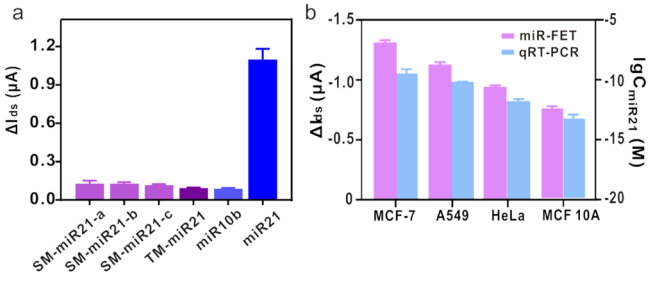

Figure 4. Specificity. (a) Selective response of the sensor toward the fully matched sequence, single-mismatched sequences at different locations, three-mismatched sequences, and unmatched miR10b. The concentration of the target miR21 is 100 fM and the concentration of other miRNAs is 1 pM. $V_{ds} = -0.1$ V and $V_g = -0.7$ V. (b) Using qRT-PCR (blue) and the miR-FET (purple) to detect different miRA21 expression levels in the total exosomal RNA isolated from three types of human cancer cell lines and a normal human mammary epithelial cell line. Error bars represent the standard errors ($n = 5$).

https://doi.org/10.1021/acs.analchem.1c03573
Anal. Chem. 2021, 93, 15501−15507

pM) were negligible, less than 15% of that by miR21 (lower concentration, 100 fM). This data clearly demonstrates the high specificity of the miR-FET sensor. The weak response to mismatched sequences is mainly attributed to nonspecific physical adsorption of the miRNAs.

In order to further prove the specificity of the sensor, we tried to detect exosomal miRNA21 extracted from different cell lines (MCF-7 and MCF 10A from the breast, HeLa from the cervix, and A549 from the lungs). The extracted exosomes from different cell lines were characterized. Transmission electron microscopy images show that the extracted exosomal particles were well dispersed and had a typical calyx, which is consistent with the description in the literature (Figure S4a). The nanoparticle tracking analysis (NTA) results show that the size distribution of the extracted exosomes was concentrated at 125−150 nm, and the concentration was 5.8×10^{11}/mL (Figure S4b). In addition, through western blot analysis of the characteristic proteins of exosomes CD63, epithelial cell adhesion molecule (EpCAM), and TSG101, it was found that they could show clear bands, confirming their normal expression on exosomes and the successful isolation of exosomes (Figure S4c). Next, we used the DNA-functionalized CNT FET sensor to measure miRNA 21 in total RNAs extracted from MCF 10A, MCF-7, HeLa, and A549 exosomes with the same concentration (1.0×10^8/mL), respectively. As shown in Figure 4b, miRNA 21 had the highest expression level in MCF-7-derived exosomes (ΔI_{ds} = 1.33 μA), followed by A549 (ΔI_{ds} = 1.14 μA) and HeLa (ΔI_{ds} = 0.95 μA), and it had the lowest expression level in MCF 10A (ΔI_{ds} = 0.73 μA) exosomes. Among them, the largest difference from the expression level in tumor cells reached about 28% (MCF-7 vs HeLa), and the difference was about 45% from the expression level in the normal mammary epithelium. The study results show that the expression of miR-21 was detectable in all tumor exosomes with substantial variation, and elevated miR-21 expression was seen in breast cancer.

In order to verify the reliability of the sensor's detection results, we used the classic method qRT-PCR to measure the same samples and compared the results with the sensor's. It is obvious that the two results were well matched (Figure 4b), indicating the accuracy and practical application potential of the sensor.

Clinical Sample Analysis. In order to verify the applicability of the miR-FET sensor for clinical diagnosis, we extracted total exosomal RNA from 20 clinical plasma samples (10 of which were healthy individuals and 10 were clinically diagnosed as breast cancer) and then analyzed miR21. As shown in Figure 5a, the signal response of plasma samples from breast cancer patients was higher than that from healthy volunteers, indicating that the expression level of exosomal miR21 in breast cancer patients was higher. Then, we used independent samples to test the two sets of data and performed statistical analysis. The results showed that the expression level of exosomal miR21 between breast cancer patients and healthy people was significantly different (p < 0.001), indicating that our sensor can better distinguish healthy samples from patient samples (Figure 5b). In addition, we constructed a receiver operator characteristic curve (ROC) to evaluate the application ability of the test in clinical diagnosis (Figure 5c). The area under the curve of the ROC figure was AUC = 0.99, which met the standard of a reliable diagnostic test (AUC > 0.8). It proves that the expression level of exosomal miRNA21 is highly accurate in diagnosing breast

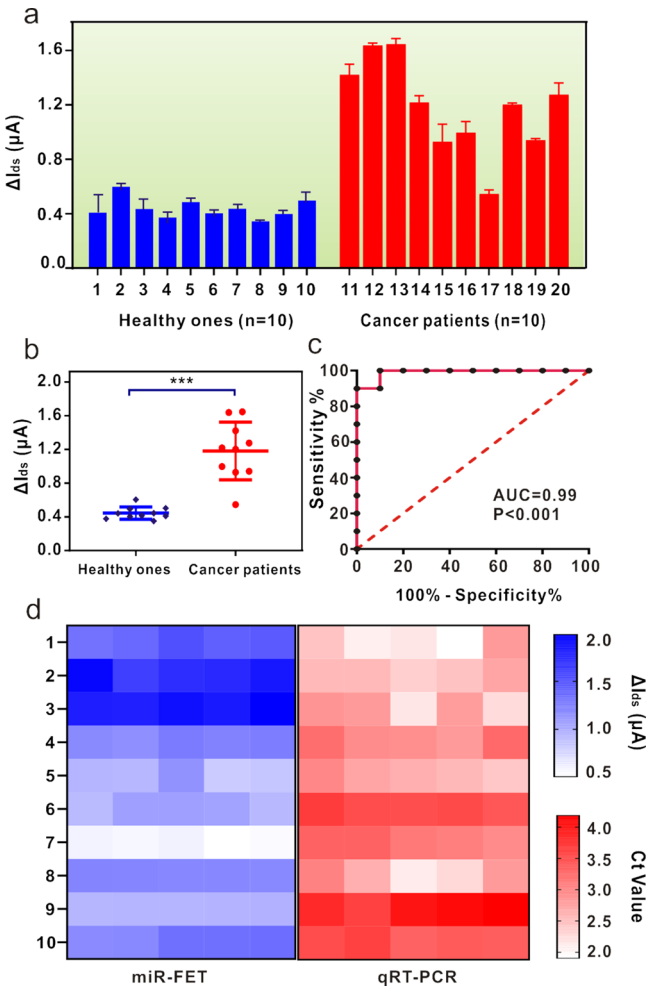

Figure 5. Clinical sample assays. (a) Using the miR-FET sensor to assay the target miR21 in circulating exosomes directly from human plasma specimens, including healthy donors (n = 10) and breast cancer patients (n = 10). (b) Significant expression difference of exosomal miR21 levels between cancer patients and healthy controls (p < 0.001). (c) ROC curve analysis shows the power to discriminate cancer patients from the normal controls by using the exosomal miR21 expression level with the miR-FET sensor. AUC is the area under the curve. Error bars represent the standard errors (n = 5). (d) Heat map depicting the degree of ΔI_{ds} (blue) and Ct value (red) across 10 clinical cancer patients. "miR-FET" indicates the results of miR-FET testing, and "qRT-PCR" indicates the results of qRT-PCR testing. Each sample is tested 5 times.

cancer patients, and exosomal miRNA21 is a potential breast cancer biomarker. In order to further verify the accuracy of the sensor detection, we tested the same sample with the standard method qRT-PCR and compared the results with the sensor's detection results. Each sample was tested 5 times to reduce accidental errors. As shown in Figure 5d, the detection results of the miR-FET sensor were consistent with the qRT-PCR detection results, proving that our miR-FET sensor can detect tumor biomarkers sensitively and specifically.

Reusability. Finally, we investigated reusability of the miR-FET biosensors. After detection, the miR-FET biosensors were treated with 8.3 M urea solution and left at room temperature for 5 min to denature the DNA−miRNA21 duplex, followed by rinsing the chip with deionized water and drying with nitrogen. By such a way, the miRNA21 was removed from the FET chip. Then, the DNA-functionalized CNT FET sensor

https://doi.org/10.1021/acs.analchem.1c03573
Anal. Chem. 2021, 93, 15501−15507

was hybridized again with the same concentration of miRNA21 under the same conditions as the first hybridization. The same process (denaturation and rehybridization) was repeated 3 times. It was found that the percentages of the second and third hybridization signal responses relative to the first one were 92.85 and 85.71% (Figure 6), respectively, indicating that the CNT FET biosensor shows a good performance in the reusability.

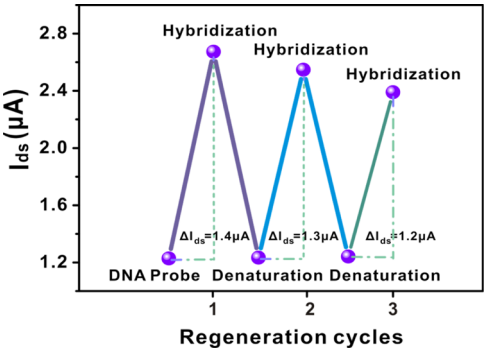

Figure 6. Reusability study of the miR-FET biosensor for exosomes miR21 detection. The concentrations of exosomes miR21 and urea were 100 pM and 8.3 M, respectively.

CONCLUSIONS

We have developed a DNA-functionalized CNT miR-FET biosensor, which can sensitively and specifically detect exosomal miRNA in a label-free manner. The CNT FET biosensor can directly convert the trace electrical signal caused by the interaction between the biomolecules of the sensing interface into a readable electrical signal, which lays the foundation for label-free detection. In addition, the miR-FET biosensor also has some outstanding advantages. First, compared with other channel materials, the high-purity semiconductor CNT network shows higher uniform performance and superior bias stress stability. Second, after modifying the Y_2O_3 insulating layer to reduce the interference of other interactions, the ultrasensitivity and specificity of the detection are ensured. Third, the miR-FET biosensor is able to distinguish the expression level of miRNA in cancer patients and healthy people, paving a way for early diagnosis of cancer. In addition, our sensor has the potential to be integrated with microfluidic technology to quickly and ultrasensitively detect multiple tumor biomarkers on one chip, thus achieving accurate diagnosis of the tumor.

ASSOCIATED CONTENT

Supporting Information

The Supporting Information is available free of charge at https://pubs.acs.org/doi/10.1021/acs.analchem.1c03573.

Sequences and involved oligonucleotide probes, performance comparison among different exosomal miRNAs sensors, energy-dispersive spectroscopy, transfer curve evolution of the miR-FET, and characterization of exosomes (PDF)

AUTHOR INFORMATION

Corresponding Authors

Wei Ni − *Hubei Provincial Hospital of Traditional Chinese Medicine, Wuhan 430061, China*; Email: niweiwh@163.com

Zhiyong Zhang − *Hunan Institute of Advanced Sensing and Information Technology, Xiangtan University, Hunan 411105, China*; orcid.org/0000-0003-1622-3447; Email: zyzhang@pku.edu.cn

Guo-Jun Zhang − *School of Laboratory Medicine, Hubei University of Chinese Medicine, Wuhan 430065, China*; orcid.org/0000-0001-9096-9226; Email: zhanggj@hbtcm.edu.cn

Authors

Tingxian Li − *School of Laboratory Medicine, Hubei University of Chinese Medicine, Wuhan 430065, China*

Yuqi Liang − *Key Laboratory for the Physics and Chemistry of Nanodevices and Center for Carbon-based Electronics, Department of Electronics, Peking University, Beijing 100871, China*

Jiahao Li − *School of Laboratory Medicine, Hubei University of Chinese Medicine, Wuhan 430065, China*

Yi Yu − *School of Laboratory Medicine, Hubei University of Chinese Medicine, Wuhan 430065, China*

Meng-Meng Xiao − *Key Laboratory for the Physics and Chemistry of Nanodevices and Center for Carbon-based Electronics, Department of Electronics, Peking University, Beijing 100871, China*

Complete contact information is available at: https://pubs.acs.org/10.1021/acs.analchem.1c03573

Notes

The authors declare no competing financial interest.

ACKNOWLEDGMENTS

This work was supported by the National Natural Science Foundation of China (21974035).

REFERENCES

(1) Bray, F.; Ferlay, J.; Soerjomataram, I.; Siegel, R. L.; Torre, L. A.; Jemal, A. *Ca-Cancer J. Clin.* **2018**, *68*, 394−424.

(2) Mattiuzzi, C.; Lippi, G. *J. Epidemiol. Glob. Health* **2019**, *9*, 217−222.

(3) Oeffinger, K. C.; Fontham, E. T. H.; Etzioni, R.; Herzig, A.; Michaelson, J. S.; Shih, Y.-C. T.; Walter, L. C.; Church, T. R.; Flowers, C. R.; LaMonte, S. J.; Wolf, A. M. D.; DeSantis, C.; Lortet-Tieulent, J.; Andrews, K.; Manassaram-Baptiste, D.; Saslow, D.; Smith, R. A.; Brawley, O. W.; Wender, R. *JAMA* **2015**, *314*, 1599−1614.

(4) Kashyap, D.; Kaur, H. *Life Sci.* **2020**, *246*, 117417.

(5) Yang, Z.; Liu, Z. *J. Oncol.* **2020**, *2020*, 9160905.

(6) Schnitt, S. J. *Mod. Pathol.* **2010**, *23*, S60−S64.

(7) Ashby, J.; Flack, K.; Jimenez, L. A.; Duan, Y.; Khatib, A.-K.; Somlo, G.; Wang, S. E.; Cui, X.; Zhong, W. *Anal. Chem.* **2014**, *86*, 9343−9349.

(8) Arroyo, J. D.; Chevillet, J. R.; Kroh, E. M.; Ruf, I. K.; Pritchard, C. C.; Gibson, D. F.; Mitchell, P. S.; Bennett, C. F.; Pogosova-Agadjanyan, E. L.; Stirewalt, D. L.; Tait, J. F.; Tewari, M. *Proc. Natl. Acad. Sci. U.S.A.* **2011**, *108*, 5003−5008.

(9) Abak, A.; Abhari, A.; Rahimzadeh, S. *PeerJ* **2018**, *6*, No. e4763.

(10) Desdín-Micó, G.; Mittelbrunn, M. *Cell Adhes. Migr.* **2017**, *11*, 127−134.

(11) Bullock, M.; Silva, A.; Kanlikilicer-Unaldi, P.; Filant, J.; Rashed, M.; Sood, A.; Lopez-Berestein, G.; Calin, G. *Noncoding RNAs* **2015**, *1*, 53−68.
(12) Yang, C.; Robbins, P. D. *Clin. Dev. Immunol.* **2011**, *2011*, 842849.
(13) Jafari, S. H.; Saadatpour, Z.; Salmaninejad, A.; Momeni, F.; Mokhtari, M.; Nahand, J. S.; Rahmati, M.; Mirzaei, H.; Kianmehr, M. *J. Cell. Physiol.* **2018**, *233*, 5200−5213.
(14) Goda, T.; Masuno, K.; Nishida, J.; Kosaka, N.; Ochiya, T.; Matsumoto, A.; Miyahara, Y. *Chem. Commun.* **2012**, *48*, 11942−11944.
(15) Miao, P.; Tang, Y. *CCS Chem.* **2021**, *3*, 2331−2339.
(16) Liu, P.; Qian, X.; Li, X.; Fan, L.; Li, X.; Cui, D.; Yan, Y. *ACS Appl. Mater. Interfaces* **2020**, *12*, 45648−45656.
(17) Peng, L.-M.; Zhang, Z.; Qiu, C. *Nat. Electron.* **2019**, *2*, 499−505.
(18) Zhao, J.; Liu, C.; Li, Y.; Ma, Y.; Deng, J.; Li, L.; Sun, J. *J. Am. Chem. Soc.* **2020**, *142*, 4996−5001.
(19) Jiang, S.; Li, Q.; Wang, C.; Pang, Y.; Sun, Z.; Xiao, R. *ACS Sens.* **2021**, *6*, 852−862.
(20) Yang, Y.; Kannisto, E.; Patnaik, S. K.; Reid, M. E.; Li, L.; Wu, Y. *ACS Appl. Nano Mater.* **2021**, *4*, 2806−2819.
(21) Vu, C. A.; Chen, W. Y. *Sensors* **2019**, *19*, 4214.
(22) Syu, Y.-C.; Hsu, W.-E.; Lin, C.-T. *ECS J. Solid State Sci. Technol.* **2018**, *7*, Q3196−Q3207.
(23) Panahi, A.; Sadighbayan, D.; Forouhi, S.; Ghafar-Zadeh, E. *Biosensors* **2021**, *11*, 103.
(24) Lahir, Y. K.; Samant, M.; Dongre, P. M. *Global J. Biosci. Biotechnol.* **2016**, *5*, 146−163.
(25) Sadighbayan, D.; Hasanzadeh, M.; Ghafar-Zadeh, E. *TrAC Trends Anal. Chem.* **2020**, *133*, 116067.
(26) Sedki, M.; Shen, Y.; Mulchandani, A. *Biosens. Bioelectron.* **2021**, *176*, 112941.
(27) Hwang, M. T.; Heiranian, M.; Kim, Y.; You, S.; Leem, J.; Taqieddin, A.; Faramarzi, V.; Jing, Y.; Park, I.; van der Zande, A. M.; Nam, S.; Aluru, N. R.; Bashir, R. *Nat. Commun.* **2020**, *11*, 1543.
(28) Song, P.; Fu, H.; Wang, Y.; Chen, C.; Ou, P.; Rashid, R. T.; Duan, S.; Song, J.; Mi, Z.; Liu, X. *Biosens. Bioelectron.* **2021**, *190*, 113264.
(29) Hills, G.; Lau, C.; Wright, A.; Fuller, S.; Bishop, M. D.; Srimani, T.; Kanhaiya, P.; Ho, R.; Amer, A.; Stein, Y.; Murphy, D.; Chandrakasan, A.; Shulaker, M. M. *Nature* **2019**, *572*, 595−602.
(30) Balasubramanian, K.; Kern, K. *Adv. Mater.* **2014**, *26*, 1154−1175.
(31) Münzer, A. M.; Michael, Z. P.; Star, A. *ACS Nano* **2013**, *7*, 7448−7453.
(32) Hu, P.; Zhang, J.; Li, L.; Wang, Z.; O'Neill, W.; Estrela, P. *Sensors* **2010**, *10*, 5133−5159.
(33) Ménard-Moyon, C.; Kostarelos, K.; Prato, M.; Bianco, A. *Chem. Biol.* **2010**, *17*, 107−115.
(34) Ko, J. W.; Woo, J.-M.; Jinhong, A.; Cheon, J. H.; Lim, J. H.; Kim, S. H.; Chun, H.; Kim, E.; Park, Y. J. *ACS Nano* **2011**, *5*, 4365−4372.
(35) Maehashi, K.; Katsura, T.; Kerman, K.; Takamura, Y.; Matsumoto, K.; Tamiya, E. *Anal. Chem.* **2007**, *79*, 782−787.
(36) Sorgenfrei, S.; Chiu, C. Y.; Gonzalez, R. L.; Yu, Y. J.; Kim, P.; Nuckolls, C.; Shepard, K. L. *Nat. Nanotechnol.* **2011**, *6*, 126−132.
(37) Zheng, H. Y.; Alsager, O. A.; Wood, C. S.; Hodgkiss, J. M.; Plank, N. O. V. *J. Vac. Sci. Technol., B: Nanotechnol. Microelectron.: Mater., Process., Meas., Phenom.* **2015**, *33*, 06F904.
(38) Gui, E. L.; Li, L.-J.; Zhang, K.; Xu, Y.; Dong, X.; Ho, X.; Lee, P. S.; Kasim, J.; Shen, Z. X.; Rogers, J. A.; Mhaisalkar, S. G. *J. Am. Chem. Soc.* **2007**, *129*, 14427−14432.
(39) Dong, X.; Lau, C. M.; Lohani, A.; Mhaisalkar, S. G.; Kasim, J.; Shen, Z.; Ho, X.; Rogers, J. A.; Li, L.-J. *Adv. Mater.* **2008**, *20*, 2389−2393.
(40) Liang, Y.; Xiao, M.; Wu, D.; Lin, Y.; Liu, L.; He, J.; Zhang, G.; Peng, L.-M.; Zhang, Z. *ACS Nano* **2020**, *14*, 8866−8874.

https://doi.org/10.1021/acs.analchem.1c03573
Anal. Chem. 2021, 93, 15501−15507